Heterogeneous alpha-cell population modeling of glucose-induced inhibition of electrical activity

Francesco Montefusco[a,*], Giuliana Cortese[b], Morten G. Pedersen[a,c,d,*]

[a] *Department of Information Engineering, University of Padova, Padova, Italy*
[b] *Department of Statistical Sciences, University of Padova, Padova, Italy*
[c] *Department of Mathematics "Tullio Levi-Civita", University of Padova, Padova, Italy*
[d] *Padova Neuroscience Center, University of Padova, Padova, Italy*

Abstract

Glucagon release from the pancreatic alpha-cells is regulated by glucose, but the underlying mechanisms are far from understood. It is known that the alpha-cell population is very heterogeneous, but – compared to the insulin-secreting beta-cells – the consequences of this cell-to-cell variation are much less studied. Since the alpha-cells are not electrically coupled, large differences in the single cell responses are to be expected, and this variation may contribute to the confusion regarding the mechanisms of glucose-induced suppression of glucagon release. Using mathematical modeling of alpha-cells with realistic cell-to-cell parameter variation based on recent experimental results, we show that the simulated alpha-cells exhibit great diversity in their electrophysiological behavior. To robustly reproduce experimental recordings from alpha-cell exposed to a rise in glucose levels, we must assume that both intrinsic mechanisms and paracrine signals contribute to glucose-induced changes in electrical activity. Our simulations suggest that the sum of different electrophysiological responses due to alpha-cell heterogeneity is involved in glucose-suppressed glucagon secretion, and that more than one mechanism contribute to control the alpha-cell populations' behavior. Finally, we apply regression analysis to our synthetic alpha-cell population to infer which membrane currents influence electrical activity in alpha-cells at different glucose levels. The results from such statistical

*Corresponding authors: montefusco@dei.unipd.it; pedersen@dei.unipd.it

modeling suggest possible disturbances underlying defect regulation of alpha-cell electrical behavior in diabetics. Thus, although alpha-cells appear to be inherently complex and heterogeneous as reflected in published data, realistic modeling of the alpha-cells at the population level provides insight into the mechanisms of glucagon release.

Keywords: Alpha-cells, heterogeneity, electrical activity, population models, regression analysis

---

1. Introduction

The islets of Langerhans forming the endocrine pancreatic system are mainly composed of alpha-, beta- and delta-cells, which secrete glucagon, insulin and somatostatin, respectively. These hormones work together to regulate glucose usage and homeostasis. At low blood glucose levels, alpha-cells secrete glucagon, which stimulates hepatic glucose output, whereas, at high glucose levels, beta-cells release insulin, which promotes glucose uptake in fat and muscles. Interestingly, it was recently shown that impaired glucagon release or disturbed paracrine alpha-to-beta-cell signaling reduce insulin secretion and glucose control (Svendsen et al. (2018); Zhu et al. (2019); Capozzi et al. (2019)). Delta-cells release somatostatin, which has an inhibitory effect on both glucagon and insulin secretion. It is now widely accepted that dysregulated pancreatic hormone secretion is involved in the development and pathophysiology of diabetes (Kahn et al. (2009); Ashcroft & Rorsman (2012); Lee et al. (2016); Rorsman & Huising (2018)).

Most studies have focused on impaired insulin secretion from beta-cells. However, glucagon release from the pancreatic alpha-cells is also disturbed in diabetes. Diabetics show excessive glucagon release at hyperglycaemia, which is generally believed to promote further stimulation of glucose output from the liver. In addition, the counter-regulatory glucagon response at hypoglycaemia, which stimulates glucose output in healthy individual to restore plasma glucose in the physiological range, is impaired in diabetes with potentially fatal

consequences (D'Alessio (2011)).

For these reasons, recent research has aimed to achieve a better understanding of regulation of glucagon secretion by glucose and other physiological factors. However, whereas the main mechanisms involved in glucose-stimulated insulin secretion from beta-cells have been well understood and established, factors regulating glucagon secretion from alpha-cells in response to glucose belong to the most contested aspects of islet cell biology generating no clear consensus (Gromada et al. (2007); Briant et al. (2016)).

Published alpha-cell data are "maddingly inconclusive" (Watts & Sherman (2014)). Glucose can sometimes depolarize (Gromada et al. (2004); Zhang et al. (2013)) or hyperpolarize (Barg et al. (2000); Manning Fox et al. (2006)) mouse alpha-cells, and, similarly, the calcium response to glucose of alpha-cells located in mouse islets can be negative (MacDonald et al. (2007); Vieira et al. (2007)) or positive (Le Marchand & Piston (2010)). Single alpha-cells can also show contrasting Ca^{2+} responses even under identical conditions (Le Marchand & Piston (2010)). In alpha-cells in human islets glucose has been reported to lower Ca^{2+} levels (Quesada et al. (2006)). These apparently conflicting results might to a large degree be explained by the tremendous heterogeneity of the alpha-cell population (Huang et al. (2011); Briant et al. (2017)). Whereas the importance of heterogeneity in the beta-cell population is generally recognized (Pipeleers (1992); Gutierrez et al. (2017); Benninger & Hodson (2018)), as reflected in several modeling studies (Smolen et al. (1993); Pedersen et al. (2008); Benninger et al. (2014); Cappon & Pedersen (2016), the role of cell-to-cell variation between alpha-cells has been studied less (but see e.g. Watts & Sherman (2014); Huang et al. (2011); Hughes et al. (2018)). Likely, the lack of clear conclusions regarding the mechanisms of glucose-induced suppression of glucagon release is a direct result of the natural alpha-cell heterogeneity.

It is established that glucagon secretion is stimulated at low glucose levels (1 mM, Gromada et al. (2007)), but there are several hypotheses trying to explain the glucose-induced inhibition of glucagon secretion at physiological levels (6 mM). An important role of somatostatin for inhibiting glucagon

secretion at physiological glucose levels is suggested for example by the fact that glucagon release is increased in somatostatin receptor 2 (SSTR2) knockout islets (Briant et al. (2016)). However, although blocking somatostatin signaling increases glucagon secretion, it does not prevent inhibition of glucagon release by glucose (Vieira et al. (2007); Cheng-Xue et al. (2013)), suggesting an important role for direct, intrinsic regulation of glucagon release. Several alternative theories have been proposed for explaining intrinsic glucagon regulation by glucose. One proposal suggests that glucose leads to closure of ATP-sensitive K^+(KATP)-channels resulting in a slight membrane depolarization, which prevents full action potential generation needed for complete activation of high voltage-activated (HVA) Ca^{2+} channels (CaVs) involved in exocytosis (Zhang et al. (2013); MacDonald et al. (2007); Göpel et al. (2000); Walker et al. (2011)). Another proposal (Vieira et al. (2007); Liu et al. (2004)) claims that glucose stimulates Ca^{2+} uptake into the endoplasmic reticulum (ER), which terminates a store-operated current (SOC) leading to membrane hyperpolarization. Sodium-glucose co-transport via the SGLT2 transporter has also been suggested to contribute to inhibition of glucagon release (Bonner et al. (2015); Pedersen et al. (2016)). A recent hypothesis that is gaining increasing support suggests that electrical activity and Ca^{2+} increases are only permissive factors for glucagon release, and that glucose inhibits secretion from alpha-cells by lowering intracellular cAMP levels (Hughes et al. (2018); Tengholm & Gylfe (2017); Yu et al. (2019)). However, the mechanisms underlying the reduction in cAMP concentration and the downstream effects on secretion are still to be established.

Mathematical modelling could provide a tool to grasp and handle these disparate results and understand better the delicate and complex system of the endocrine pancreas, in particular the alpha-cells. Diderichsen & Göpel (2006) developed a mathematical model of electrical activity based on ion channel characteristics of alpha-cells located on the surface of intact mouse islet. Watts & Sherman (2014) presented an updated version of the model by including Ca^{2+} dynamics and secretion, and modifying ionic currents with the aim to achieve a better agreement with experimental data (by reducing spike frequency and in-

creasing spike amplitude). We modified the model of Watts & Sherman (2014) by devising a detailed model of Ca^{2+} dynamics and exocytosis (Montefusco & Pedersen (2015)), in particular, by carefully describing the Ca^{2+} levels near open or closed Ca^{2+} channels of various types and their contribution to control of glucagon secretion in response to glucose and hormones (such as adrenaline and GLP-1), clarifying why cytosolic Ca^{2+} may be a poor read-out of alpha-cell secretion. Pedersen et al. (2016) developed a mathematical model of alpha-cell electrical activity based on published data from human alpha-cells, explaining how SLGT2 currents might affect the shape of alpha-cell action potential and its inhibitory effect on glucagon secretion at high glucose levels, as experimentally observed (Bonner et al. (2015); Pedersen et al. (2016)). Recently Briant et al. (2017) presented a new update of the model of Watts & Sherman (2014), based on their experimental findings, with the aim to improve the fit to the experimental data, in particular, the spike amplitude at low and at physiological glucose levels.

However, all the models developed so far describe a single alpha-cell, providing at most an "average" description of the entire population without considering the large and well described experimental heterogeneity of the population (Huang et al. (2011); Briant et al. (2017)). Here, we will systematically take this cell-to-cell variation into account, respecting published data on the different currents and the capacitance from single alpha-cells (Huang et al. (2011); Briant et al. (2017)), in order to reproduce the disparate and apparently contrasting electrophysiological responses at similar conditions. In this way, we will achieve a realistic description of the entire alpha-cell population rather than of an "average" alpha-cell. Having a holistic description of cell-to-cell heterogeneity allows us to perform statistical regression analysis of the simulation results, which enable us to predict the role of the various membrane currents in controlling electrical activity in a realistic synthetic alpha-cell population. The obtained results suggest possible electrophysiological disturbances in diabetic alpha-cells.

2. Methods

2.1. Single alpha-cell electrical activity model

The alpha-cell electrical activity is simulated by including all the relevant ion currents for which experimental data are available (Huang et al. (2011); Briant et al. (2017); Diderichsen & Göpel (2006)), following previous modeling (Watts & Sherman (2014); Diderichsen & Göpel (2006); Montefusco & Pedersen (2015)). In particular, we assume a low-threshold voltage activated (LVA) T-type Ca^{2+} current, I_{CaT}, two types of high voltage-activated (HVA) Ca^{2+} currents, the L-type Ca^{2+} and the P/Q-type currents, I_{CaL} and $I_{CaP/Q}$, a voltage-dependent Na^{+} current, I_{Na}, a delayed rectifier K^{+} current, I_K, an A-type voltage-dependent K^{+} current, I_{KA}, an ATP-sensitive K^{+} current, I_{KATP}, a leak current, I_L, and G-protein coupled inwardly rectifying K^{+} (GIRK) current, I_{GIRK}, activated by somatostatin. Therefore, the membrane potential, V, is given by the following ODE:

$$\frac{dV}{dt} = -\left(I_{CaT} + I_{CaL} + I_{CaP/Q} + I_{Na} + I_K + I_{KA} + I_{KATP} + I_L + I_{GIRK}\right). \tag{1}$$

The currents normalized by membrane capacitance, C_m, in Eq. (1) are described by

$$I_{CaT} = \tilde{g}_{CaT} m_{CaT}^3 h_{CaT} (V - V_{Ca}), \tag{2}$$

$$I_{CaL} = \tilde{g}_{CaL} m_{CaL}^2 h_{CaL} (V - V_{Ca}), \tag{3}$$

$$I_{CaP/Q} = \tilde{g}_{CaP/Q} m_{CaP/Q} h_{CaP/Q} (V - V_{Ca}), \tag{4}$$

$$I_{Na} = \tilde{g}_{Na} m_{Na}^3 h_{Na} (V - V_{Na}), \tag{5}$$

$$I_K = \tilde{g}_K m_K^4 (V - V_K), \tag{6}$$

$$I_{KA} = \tilde{g}_{KA} m_{KA} h_{KA} (V - V_K), \tag{7}$$

$$I_{KATP} = \tilde{g}_{KATP} (V - V_K), \tag{8}$$

$$I_L = \tilde{g}_L (V - V_L), \tag{9}$$

$$I_{GIRK} = \tilde{g}_{GIRK} (V - V_K), \tag{10}$$

where $\tilde{g}_x$ represents the conductance density of the channel x (i.e the channel conductance, g_x, scaled by C_m, $\tilde{g}_x = g_x/C_m$) and V_{Ca}, V_{Na}, V_K, V_L the reverse potentials. m_x and h_x are, respectively, the activation and inactivation variables of channel x and are given as:

$$\frac{dm_x}{dt} = \frac{m_{x,\infty}(V) - m_x}{\tau_{m_x}(V)}, \tag{11}$$

$$\frac{dh_x}{dt} = \frac{h_{x,\infty}(V) - h_x}{\tau_{h_x}(V)}, \tag{12}$$

where $m_{x,\infty}$ and $h_{x,\infty}$ are the steady state activation and inactivation curves, respectively, and τ_{m_x} and τ_{h_x} the time-constants for m_x and h_x, respectively. The steady state activation and inactivation curves are described with Boltzmann functions,

$$m_{x,\infty}(V) = \frac{1}{1 + \exp\left(-\frac{V - V_{m_x}}{S_{m_x}}\right)}, \tag{13}$$

$$h_{x,\infty}(V) = \frac{1}{1 + \exp\left(-\frac{V - V_{h_x}}{S_{h_x}}\right)}, \tag{14}$$

while the time constants are bell shaped functions,

$$\tau_{m_x}(V) = \frac{\tau_{m_{V_x}}}{\exp\left(-\frac{V - V_{\tau_{m_x}}}{S_{\tau_{m_x}}}\right) + \exp\left(\frac{V - V_{\tau_{m_x}}}{S_{\tau_{m_x}}}\right)} + \tau_{m_{0_x}}, \tag{15}$$

$$\tau_{h_x}(V) = \frac{\tau_{h_{V_x}}}{\exp\left(-\frac{V - V_{\tau_{h_x}}}{S_{\tau_{h_x}}}\right) + \exp\left(\frac{V - V_{\tau_{h_x}}}{S_{\tau_{h_x}}}\right)} + \tau_{h_{0_x}}. \tag{16}$$

2.2. Heterogeneous alpha-cell population model

For a typical parameter set, the single alpha-cell model defined by Eq. (1) gives an "average" description of the entire population without taking the tremendous heterogeneity of the population (Huang et al. (2011); Briant et al. (2017)) into account. We exploited the experimental data from individual alpha-cells on cell capacitance, the whole-cell input conductance, the maximum sodium current and the maximum calcium current for LVA and HVA channels. In particular, we simulated the electrical behavior of an alpha-cell population of one-thousand cells by varying the parameters describing the electrical property

of each single cell defined by Eq. (1) according to the experimental findings. Thus, for each cell we randomly extracted its electrophysiological parameters from experimentally characterized distributions (Huang et al. (2011); Briant et al. (2017)). Briant et al. (2017) provided the investigated parameters for the individual, patched cells, not only as distributions, which allowed us to study whether any correlation between the different parameters were present, as one might have expected. Indeed, we found low, but significant, correlation between the cell capacitance, C_m, and the absolute value of maximum sodium current density, $|I_{Na_{max}}|$ (see Supplementary Fig. S1). Moreover, by distinguishing alpha-cells with and without A-type K^+ current, we observed that cells with such a current were characterized by larger whole-cell input conductance density, $\tilde{G}$, values than those reported for the cells without A-current. Therefore, we computed the parameter distributions from the data-set reported in Briant et al. (2017) by fitting the experimental data and taking into account the significant correlations: we obtained lognormal distributions for C_m and $|I_{Na_{max}}|$ and the resulting correlated distribution; we computed two lognormal distributions for $\tilde{G}$ by assuming the presence or absence of A-type K^+current, $\tilde{G}_{A_{ON}}$ and $\tilde{G}_{A_{OFF}}$, respectively, and introduced a boolean variable f_{KA} indicating the presence of such a current (in 10% of alpha-cells, based on 14 of 141 cells in the dataset in Briant et al. (2017)). Based on the experimental findings reported in Zhang et al. (2013), we estimated that 25% of the $\tilde{G}$ conductance value represents the KATP-channel conductance density, $\tilde{g}_{KATP}$, while the leak conductance density value, $\tilde{g}_L$ was set to 50% of $\tilde{G}$. From the absolute value of the maximum sodium current density we got an estimation of the Na^+ channel conductance density $\tilde{g}_{Na}$.

From the experimental data reported in Huang et al. (2011), we obtained lognormal distributions for the absolute values of maximum LVA Ca^{2+} current density, $|I_{LVACa_{max}}|$, which provided an estimation of the T-type Ca^{2+} channel conductance density, $\tilde{g}_{CaT}$, and of maximum HVA Ca^{2+} current density, $|I_{HVACa_{max}}|$, which provided an estimation of the P/Q-type and L-type Ca^{2+} channel conductance densities, $\tilde{g}_{CaP/Q}$ and $\tilde{g}_{CaL}$ (see Supplementary Fig. S1).

For the K^+ currents, we used the conductance $g_K = 4.5$ pS as Watts & Sherman (2014). The cell specific K^+ conductance density $\tilde{g}_K$ was obtained by dividing g_K by C_m for each cell, thus introducing cellular heterogeneity for the K^+ current. Note that higher values of C_m correspond to smaller K^+ currents compared to the other currents, as these were generated from distributions of conductance densities and therefore independently of the C_m value.

For the activation and inactivation functions defined above, we used the parameters presented in the recent model devised by Watts & Sherman (2014) with few changes. In particular, we modified the parameters of the steady state activation curve of the P/Q-type Ca^{2+} channels as performed in our recent work (Montefusco & Pedersen (2015)), by taking into account the voltage dependence of exocytosis (Zhang et al. (2013)). We also modified the steady-state Na^+ current inactivation as done in Briant et al. (2017) according to their experimental data on Na^+ currents. The resulting alpha-cell system is named *model 1*.

Finally, we simulated the electrical behavior of the alpha-cell population by using the parameter values reported in the first developed alpha-cell model for the activation and inactivation functions (Diderichsen & Göpel (2006), named *model 2*). Table 1 reports the fixed and randomly extracted parameters used for simulating the electrical behavior of alpha-cell population at low glucose levels (1 mM, denoted G1) for *model 1* and *model 2*. The table also specifies the parameter variations modeling the transition from low (G1) to physiological glucose levels (6 mM, denoted G6), as explained in the next section.

2.3. Modelling glucose effects

We simulate four different cases for reproducing the effects due to a glucose increase from low (G1) to physiological (G6) glucose levels (see also Table 2 reporting a schematic representation of the parameter variations for the different cases).

In all four cases, we simulate the transition by decreasing the KATP-channel conductances by 20% (Gromada et al. (2004); Zhang et al. (2013)). In *case 1*, we only modify the KATP-channel conductance. In *case 2*, we also increase

Table 1: **Alpha-cell population model parameters**

Variable parameters				
Parameters	Distributions	Values	Units	Obtained parameters
C_m $\lvert I_{Na_{max}}\rvert$	multivariate lognormal $\left(\mu_{C_m}, \mu_{I_{Na_{max}}}, \sigma^2_{C_m}, \sigma^2_{I_{Na_{max}}}, \rho\right)$	$\mu_{C_m} = 1.4$, $\sigma_{C_m} = 0.27$ $\mu_{I_{Na_{max}}} = 4.64$ $\sigma_{I_{Na_{max}}} = 0.43$ $\rho = -0.2$	pF pA pF^{-1} pA pF^{-1}	$\tilde{g}_K = \frac{g_K}{C_m}$ $\tilde{g}_{KA} = \frac{g_{KA}}{C_m}$ $\tilde{g}_{GIRK} = \frac{g_{GIRK}}{C_m}$ $\tilde{g}_{Na} = \frac{\lvert I_{Na_{max}}\rvert}{-(V_{Na_{max}}{}^{(a)} - V_{Na})}$
$\tilde{G}_{A_{ON}}$	lognormal $\left(\mu_{\tilde{G}_{A_{ON}}}, \sigma^2_{\tilde{G}_{A_{ON}}}\right)$	$\mu_{\tilde{G}_{A_{ON}}} = -0.83$ $\sigma_{\tilde{G}_{A_{ON}}} = 0.28$	nS pF^{-1}	$\tilde{g}_{KATP} = 0.25 \cdot \tilde{G}_{A_{ON}}$ $\tilde{g}_L = 0.5\,\tilde{G}_{A_{ON}}$
$\tilde{G}_{A_{OFF}}$	lognormal $\left(\mu_{\tilde{G}_{A_{OFF}}}, \sigma^2_{\tilde{G}_{A_{OFF}}}\right)$	$\mu_{\tilde{G}_{A_{OFF}}} = -2.09$ $\sigma_{\tilde{G}_{A_{OFF}}} = 0.89$	nS pF^{-1}	$\tilde{g}_{KATP} = 0.25 \cdot \tilde{G}_{A_{OFF}}$ $\tilde{g}_L = 0.5\,\tilde{G}_{A_{OFF}}$
$\lvert I_{LVACa_{max}}\rvert$	lognormal $\left(\mu_{I_{LVACa_{max}}}, \sigma^2_{I_{LVACa_{max}}}\right)$	$\mu_{I_{LVACa_{max}}} = 2.07$ $\sigma_{I_{LVACa_{max}}} = 0.41$	pA pF^{-1}	$\tilde{g}_{CaT} = \frac{\lvert I_{LVACa_{max}}\rvert}{-(V_{LVACa_{max}}{}^{(b)} - V_{Ca})}$
$\lvert I_{HVACa_{max}}\rvert$	lognormal $\left(\mu_{I_{HVACa_{max}}}, \sigma^2_{I_{HVACa_{max}}}\right)$	$\mu_{I_{HVACa_{max}}} = 2.19$ $\sigma_{I_{HVACa_{max}}} = 0.39$	pA pF^{-1}	$\tilde{g}_{HVCa} = \frac{\lvert I_{HVACa_{max}}\rvert}{-(V_{HVACa_{max}}{}^{(c)} - V_{Ca})}$ $\tilde{g}_{CaL} = \tilde{g}_{HVCa} \cdot 0.8 \cdot 1.05$ [(d)] $\tilde{g}_{CaP/Q} = \tilde{g}_{HVCa} \cdot 0.2 \cdot 2$
f_{KA}	$f_{KA} \in \{0, 1\}$, $\mathrm{pr}(0) = 0.9$, $\mathrm{pr}(1) = 0.1$			$\tilde{g}_{KA} = f_{KA} \cdot \tilde{g}_{KA}$

Fixed parameters							
Parameters	Values	Parameters	Values	Parameters	Values	Parameters	Values
V_{Ca}	65 mV	V_{Na}	110 mV	V_K	-75 mV	V_L	-25 mV
$S_{m_{CaT}}$	4 mV	$S_{h_{CaT}}$	-5 mV	$\tau_{m_{0_{CaT}}}$	0 ms	$V_{\tau_{m_{CaT}}}$	-50 mV
$S_{\tau_{m_{CaT}}}$	12 mV	$\tau_{h_{V_{CaT}}}$	20 ms	$\tau_{h_{0_{CaT}}}$	5 ms	$V_{\tau_{h_{CaT}}}$	-50 mV
$S_{\tau_{h_{CaT}}}$	15 mV	$S_{m_{CaL}}$	10 mV	$S_{h_{CaL}}$	-5 mV	$\tau_{m_{V_{CaL}}}$	1 ms
$\tau_{m_{0_{CaL}}}$	0.05 ms	$V_{\tau_{m_{CaL}}}$	-23 mV	$S_{\tau_{m_{CaL}}}$	20 mV	$V_{\tau_{h_{CaL}}}$	0 mV
$S_{\tau_{h_{CaL}}}$	20 mV	$V_{m_{CaP/Q}}$	-1 mV	$S_{m_{CaP/Q}}$	4 mV	$V_{h_{CaP/Q}}$	-33 mV
$S_{h_{CaP/Q}}$	-5 mV	$\tau_{m_{V_{CaP/Q}}}$	1 ms	$\tau_{m_{0_{CaP/Q}}}$	0.05 ms	$V_{\tau_{m_{CaP/Q}}}$	-23 mV
$S_{\tau_{m_{CaP/Q}}}$	20 mV	$\tau_{h_{V_{CaP/Q}}}$	60 ms	$\tau_{h_{0_{CaP/Q}}}$	51 ms	$V_{\tau_{h_{CaP/Q}}}$	0 mV
$S_{\tau_{h_{CaP/Q}}}$	20 mV	$S_{m_{Na}}$	4 mV	$V_{h_{Na}}$	-38 mV	$S_{h_{Na}}$	-4 mV
$\tau_{m_{V_{Na}}}$	6 ms	$\tau_{m_{0_{Na}}}$	0.05 ms	$V_{\tau_{m_{Na}}}$	-50 mV	$S_{\tau_{m_{Na}}}$	10 mV
$\tau_{h_{0_{Na}}}$	0.5 ms	$V_{\tau_{h_{Na}}}$	-50 mV	$S_{\tau_{h_{Na}}}$	8 mV	S_{m_K}	23 mV
$\tau_{m_{V_K}}$	1.5 ms	$\tau_{m_{0_K}}$	15 ms	$V_{\tau_{m_K}}$	-10 mV	$S_{\tau_{m_K}}$	25 mV
$S_{m_{Ka}}$	10 mV	$V_{h_{Ka}}$	-68 mV	$\tau_{m_{V_{Ka}}}$	0 ms	$V_{\tau_{h_{Ka}}}$	5 mV
$S_{\tau_{h_{Ka}}}$	20 mV						

Fixed parameters for models 1 and 2							
Parameters	Values for model 1 (2)	Parameters	Values for model 1 (2)	Parameters	Values for model 1 (2)	Parameters	Values for model 1 (2)
g_K	4.5 (4.9) pF	g_{KA}	1 (20) pF	$V_{m_{CaT}}$	-49 (-44) mV	$V_{h_{CaT}}$	-52 (-46) mV
$\tau_{m_{V_{CaT}}}$	15 (40) ms	$V_{m_{CaL}}$	-30 (-25) mV	$V_{h_{CaL}}$	-33 (-28) mV	$\tau_{h_{V_{CaL}}}$	60 (30) ms
$\tau_{h_{0_{CaL}}}$	51 (21) ms	$V_{m_{Na}}$	-30 (-25) mV	$\tau_{h_{V_{Na}}}$	120 (80) ms	V_{m_K}	-25 (-18.5) mV
$V_{m_{Ka}}$	-45 (0) mV	$S_{h_{Ka}}$	-10 (-4) mV	$\tau_{m_{0_{Ka}}}$	0.1 (0.5) ms	$\tau_{h_{V_{Ka}}}$	60 (30) ms
$\tau_{h_{0_{Ka}}}$	5 (21) ms						

Parameter variations from G1 to G6				
Parameters in G1	Parameters in G6			
	Case 1	Case 2	Case 3	Case 4
$\tilde{g}_{KATP}$	$0.8\,\tilde{g}_{KATP}$	$0.8\,\tilde{g}_{KATP}$	$0.8\,\tilde{g}_{KATP}$	$0.8\,\tilde{g}_{KATP}$
$\tilde{g}_L$	$\tilde{g}_L$	$2\,\tilde{g}_L$	$\tilde{g}_L$	$2\,\tilde{g}_L$
- ($g_{GIRK} = 0$ nS)	-	-	$g_{GIRK_{max}}$ (= 0.15 nS)	$g_{GIRK_{max}}$

[(a)] The Na^+maximum current is at about 0 mV. [(b)] The LVA Ca^{2+}maximum current is at about -26 mV. [(c)] The HVA Ca^{2+}maximum current is at about 0 mV. [(d)] We assume that the 80% of HVA Ca^{2+}currents is L-type, while the remaining P/Q-type (Rorsman et al. (2012)). Moreover, at 0 mV, which is the voltage value for the HVA Ca^{2+}peak, the L-type Ca^{2+}channels are almost all activated (about 90-95%), while the P/Q-type Ca^{2+}channels are half-activated.

Table 2: **Representation of the model parameter variations modeling glucose increase and their effects on electrophysiological responses for the different simulated cases.**

Case	Parameter variations			Electrophysiological responses		
	$\tilde{g}_{KATP}$	$\tilde{g}_{L}$	$\tilde{g}_{GIRK}$	AP lowering	EA $\rightarrow$ Hy	Hy $\rightarrow$ De/EA
1	$\downarrow$	-	-	-	-	✓
2	$\downarrow$	$\uparrow$	-	✓	-	✓
3	$\downarrow$	-	$\uparrow$	-	✓	-
4	$\downarrow$	$\uparrow$	$\uparrow$	✓	✓	✓

the leak conductance by 2 times of its default value as similarly performed in Montefusco & Pedersen (2015). In *case 3*, we introduce a GIRK current that models the effects of somatostatin on alpha-cell regulation (Briant et al. (2016)) and we simulate the transition from G1 to G6 by increasing the GIRK channel conductance from 0 nS to its maximum value, $g_{GIRK_{max}} = 0.15$ nS, which is scaled for each cell by C_m. Finally, in *case 4*, we combine the previous parameter variations, by decreasing the KATP-channel conductance and increasing the leak and GIRK channel conductance values.

2.4. Availability of models and computer code

MATLAB files containing the code for generating the simulated alpha-cell populations presented in this work are provided as a zipped folder in the Supplementary Material.

2.5. Statistical analysis

We studied the 1000 cells simulated by G1 and G6 under *model 1*, *case 4* by regression analysis. We considered three samples: cells at G1; cells at G6; the subgroup of 770 cells, which exhibited electrical activity (EA) under 1 mM glucose, at G6. We fitted a multinomial logistic model for the response variable with three categories (based on three different electrical behaviors observed in the simulated populations, see Results and Fig. 1): electrical activity (EA), hyperpolarization (Hy) and depolarization (De). The parameters f_{KA} and log-transformed C_m, $\tilde{G}$, $|I_{Na_{max}}|$, $|I_{LVACa_{max}}|$ and $|I_{HVACa_{max}}|$, were inserted as

explanatory variables into the statistical model. In the analyses, the joint effect of the various parameters on the response was also investigated by testing all possible statistical interactions. The final statistical models were obtained after performing model selection based on stepwise procedures and the AIC index. Two-sided tests of hypothesis were performed at a significant level of 5%. A Wald test (z-test or t-test) was used for testing independent samples from simulated data, while the nonparametric Mann-Whitney test was applied for independent samples with small size from experimental data. To study whether the distribution of the cell population among the different electrophysiological responses changed significantly from G1 to G6, a marginal homogeneity test was used (in particular, a Madansky test of interchangeability).

All analyses were performed in R (R Core Team (2018)). In particular, multinomial regression analyses were conducted with the package `mlogit` (Croissant (2018)).

3. Results

From electrophysiological data (Huang et al. (2011); Briant et al. (2017)), it is evident that the alpha-cells show substantial heterogeneity (see Supplementary Fig. S1). We investigate these features by varying the main alpha-cell parameters according to the experimental observations (Huang et al. (2011); Briant et al. (2017)) (see Methods). We considered the possibility that some electrophysiological parameters could be correlated as a means for the cells to compensate, e.g., between different types of currents. From the cell-specific data-set provided in Briant et al. (2017), we found correlation between the cell capacitance and the maximum sodium current (see the first row of Supplementary Fig. S1). Moreover, by taking into account the presence/absence of A-type K^+current (transient outward current), we observed that the cells with A-current were characterized by larger whole-cell conductance values than those reported for the cells without A-current (see the second row of Supplementary Fig. S1). For the other electrophysiological parameters, we did not

find any correlation. Parameter distributions were therefore obtained by fitting the experimental data (see the third and fourth rows of Supplementary Fig. S1) under the assumption of the statistical correlations resulting from our analysis (see Methods).

We follow the electrophysiological-centered hypothesis that both depolarized and hyperpolarized alpha-cells secrete only basal amounts of glucagon due to the absence of action potentials needed for activation of P/Q-type Ca^{2+} channels needed for exocytosis. Similarly, we assume that reduced action potential height would result in less glucagon secretion (Zhang et al. (2013); MacDonald et al. (2007); Göpel et al. (2000); Walker et al. (2011)). We thus simulate the effects produced by glucose increase (from 1 to 6 mM) on alpha-cell electrophysiology, and distinguish between three different behaviors in terms of membrane potential (see Fig. 1): electrical activity (EA – left panel), hyperpolarization (Hy – middle-left panel) and depolarization (De – middle-right panel). In particular, we investigate which conditions allow us to reproduce the two different inhibitory scenarios produced by such a glucose increase: (i) action potentials (APs) with reduced amplitude with both reduction in action potential peak voltage and increase of the inter-spike membrane potential of about 9 mV (Zhang et al. (2013)); (ii) spontaneous repolarization, likely caused by somatostatin signaling (Briant et al. (2016)) (respectively blue and black plots in the right panel in Fig. 1).

3.1. Decreasing only the KATP-channel conductance cannot explain the inhibitory effect produced by glucose increase

Fig. 2 shows the electrical behavior of the alpha-cell population by simulating the activity of 1000 different cells at low (G1) and at physiological (G6) glucose levels, where the glucose increase is obtained by decreasing the KATP-channel conductance (see Methods). We call this scenario *case 1.*

At G1, 77% of the cells exhibit EA, 22.7% are in a silent state (Hy), while only 0.3% are depolarized (De behavior) (Figs. 2A and 2B). The distribution of the cell population among the different types of electrophysiological response

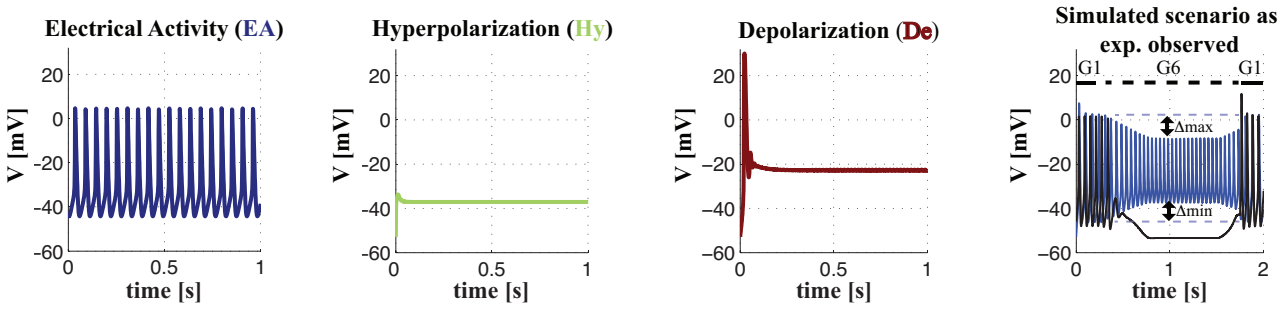

Figure 1: **Classification of simulated electrical behavior of alpha-cell population at low (G1) and physiological (G6) glucose levels.** Three different behaviors in terms of electrical activity: electrical activity (EA – left panel, blue curve), hyperpolarization (Hy – middle-left panel, green curve) and depolarization (De – middle-right panel, red curve). Simulated scenarios (right panel) due to glucose increase from 1 mM (G1) to 6 mM (G6): spike amplitude reduction (blue curve) and repolarization (black curve).

is significantly different at G6 (Figs. 2A and 2B; $p < 0.001$ by Madansky test of interchangeability). At this higher glucose concentration we observe a rise in the number of the cells with EA, since about half of cells in the silent state (Hy) become active (101 of 227 cells, Figs. 2B and 2D), while almost all the cells with EA in G1 continue to exhibit electrical behaviour (767 of 770 cells, Figs. 2B and 2C), except rare cells (3 of 770 cells) that become depolarized (Figs. 2B and 2G). The few depolarized cells in G1 remain in that state in G6 (3 cells, Figs. 2B and 2F). For the cells with EA in both G1 and G6 (767 cells, Fig. 2C), the amplitude reduction observed experimentally is not reproduced, in particular, the median reduction in action potential peak voltage is less than 1 mV, while the increase of the minimum inter-spike potential is ∼1 mV. Concerning the frequency, there is a slight increase due to the glucose effect as observed experimentally (Zhang et al. (2013)). The cells that are hyperpolarized at both glucose levels generally show a slight increase of the voltage value (126 of 227 cells, Fig. 2E). Finally, the behavior of the few depolarized cells in both G1 and G6 is very similar at both glucose concentrations (3 cells, Fig. 2F).

In summary, simulating the glucose increase from G1 to G6 by decreasing only the value of the KATP-channel conductance is insufficient to reproduce the

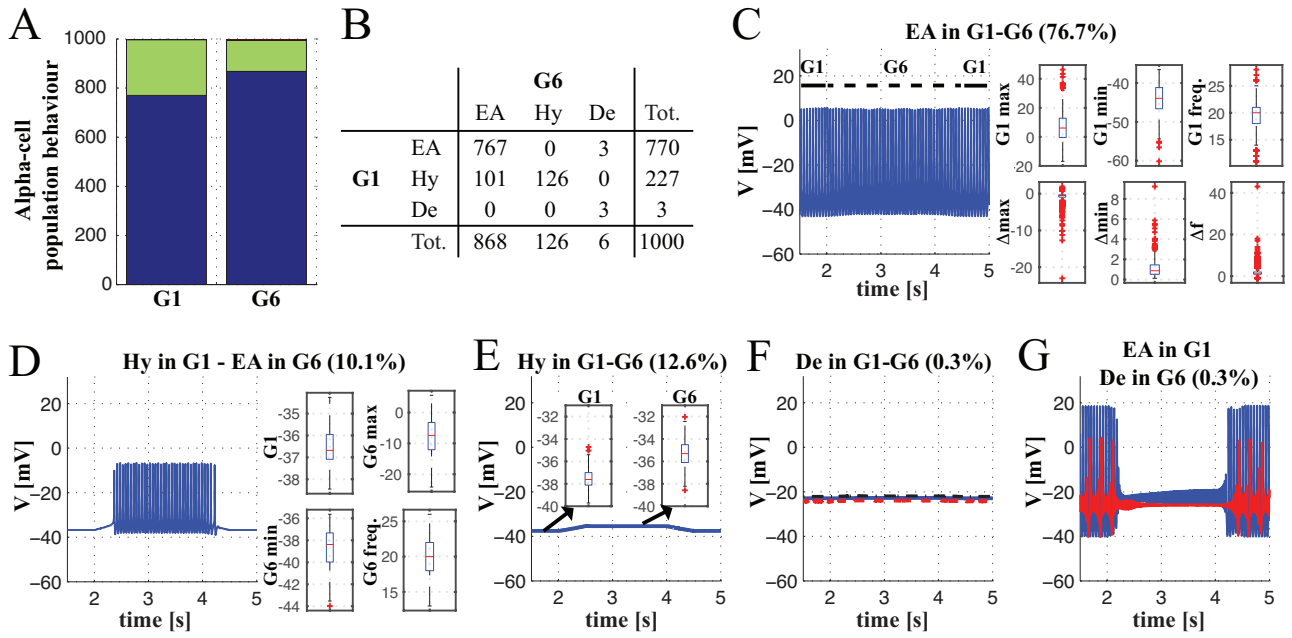

		G6			
		EA	Hy	De	Tot.
G1	EA	767	0	3	770
	Hy	101	126	0	227
	De	0	0	3	3
	Tot.	868	126	6	1000

Figure 2: **Simulated electrical behavior of alpha-cell population at low (G1) and physiological (G6) glucose levels by varying only the KATP-channel conductance for the transition from G1 to G6.** (A) Classification in terms of electrical behavior of a population of 1000 alpha-cells at G1 and G6: blue bars indicate cells with EA, green bars cells with Hy, red bars cells with De. (B) Contingency table reporting the number of cells that remain or change state (among EA, Hy, De) from G1 to G6 (or viceversa). The last column reports the total number of cells with EA, Hy and De in G1, while the last row provides the total number of cells with EA, Hy and De in G6. (C) Median behavior of cells with EA both in G1 and in G6 and boxplot representation in terms of maximum, minimum and frequency values of the spike in G1 (G1 max, G1 min, G1 freq.) and the difference between the values in G6 and G1 (Δmax = G6 max − G1 max, Δmin = G6 min − G1 min, Δf = G6 freq. − G1 freq.). (D) Median behavior of hyperpolarized cells in G1 and with EA in G6 and the corresponding boxplot representation. (E) Median behavior of hyperpolarized cells both in G1 and in G6 and the corresponding boxplot representation. (F) The behavior of the only three cells that were depolarized both in G1 and in G6. (G) The behavior of the only three cells with EA in G1 and De in G6. The convention used here and in the rest of the paper for the boxplots is as follows. The central mark indicates the median, and the bottom and top edges of the box indicate the 25th and 75th percentiles, respectively. The whiskers extend to the most extreme data points not considered outliers (defined as a value that is more than 1.5 times the interquartile range away from the top or bottom of the box), and the outliers are plotted individually with a red + symbol.

spike amplitude reduction experimentally observed. Moreover, it does not allow simulating cells exhibiting electrical behavior at low glucose levels (G1) that repolarize and become silent at physiological ones (G6). Instead, a relevant number of hyperpolarized cells become active when KATP-channel closure is simulated, in agreement with some experiments with the KATP-channel antagonist Tolbutamide (Gromada et al. (2007); Quoix et al. (2008), but see Zhang et al. (2013)). Overall, our simulations of *case 1* showed a rise in the fraction of cells exhibiting EA at physiological glucose levels, which would plausibly be reflected in increased glucagon release, in contrast to experiments.

3.2. Increasing leak conductance allows reproducing the glucose effects on electrical activity

We simulate the glucose increase by decreasing the KATP-channel conductance and increasing the leak conductance as performed in our recent work (Montefusco & Pedersen (2015)). The increased leak conductance could represent a mixture of various currents induced by glucose, for example SGLT2-mediated currents (Bonner et al. (2015); Pedersen et al. (2016)). We call this scenario *case 2*. Fig. 3A shows the electrical behavior of the 1000 different cells at low (G1) and at physiological (G6) glucose levels, as done for the previous case, with the only difference of increasing the leak conductance in G6 in addition to lowering the KATP-channel conductance (see Methods). As above, the distribution among EA, Hy and De is significantly different between G1 and G6 ($p < 0.001$ by Madansky test of interchangeability).

In this case, going from G1 to G6, we note a reduction in the fraction of cells in the silent state (hyperpolarization) and with EA, with a corresponding increase of depolarized cells (see Figs. 3B, 3F and 3G). Most of the hyperpolarized cells in G1 becomes depolarized (154 of 227 cells, see Figs. 3B and 3G), while other cells initiate electrical activity (59 of 227 cells, see Figs. 3B and 3D) counteracting partially the transition from EA to De (154 of 770 cells, see Figs. 3B and 3F). Only a few cells remain silent (14 of 227 cells, see Figs. 3B and 3E). The cells exhibiting EA both in G1 and G6 (611 cells, see Figs. 3B and 3C) are

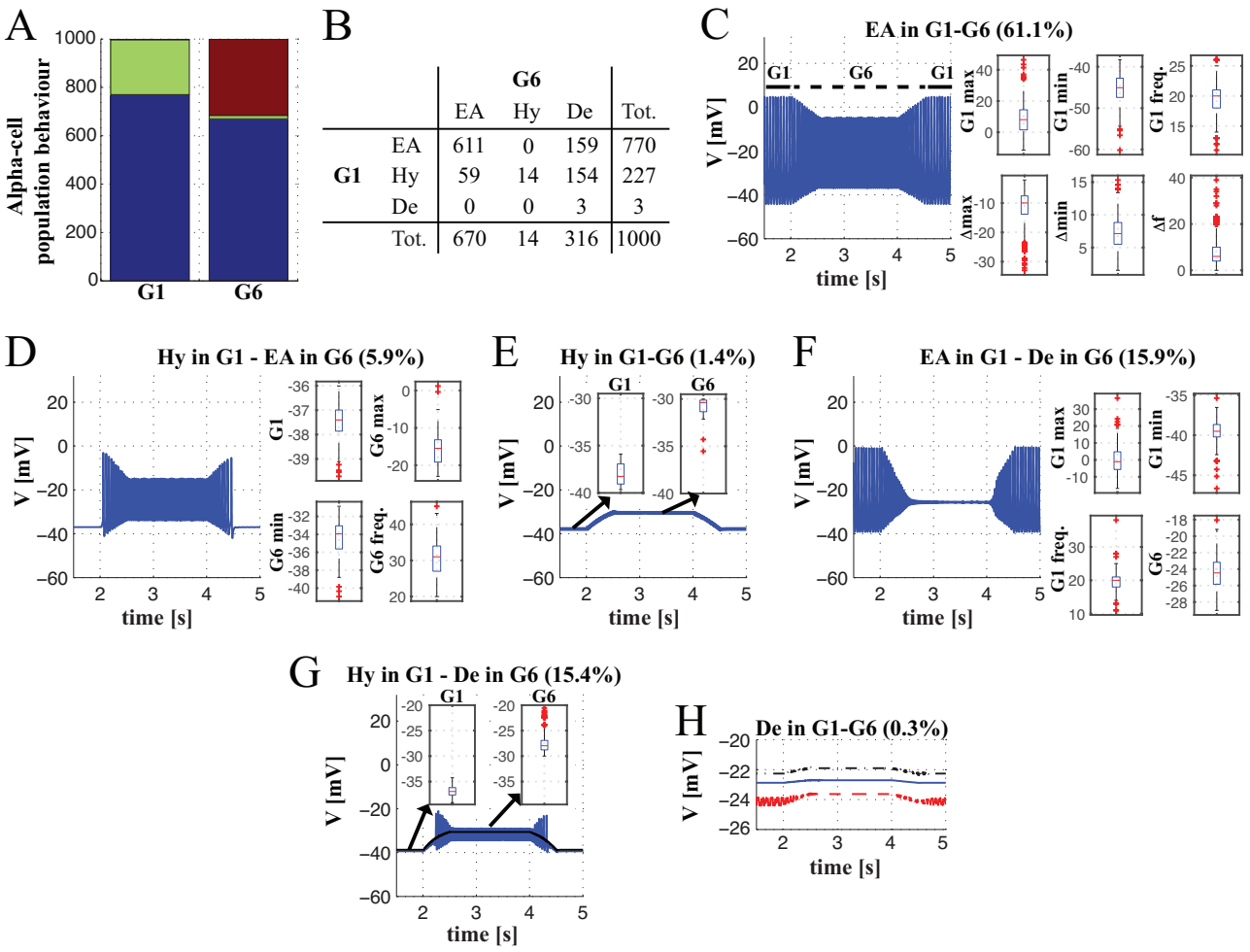

		G6			
		EA	Hy	De	Tot.
G1	EA	611	0	159	770
	Hy	59	14	154	227
	De	0	0	3	3
	Tot.	670	14	316	1000

Figure 3: **Simulated electrical behavior of alpha-cell population at low (G1) and physiological (G6) glucose levels by varying the KATP-channel and leak conductance for the transition from G1 to G6.** (A-B) Classification in terms of electrical behavior of the same population in Fig. 2 at G1 and G6 using the same criteria. (C) Median behavior of cells with EA both in G1 and in G6 and the corresponding boxplot representation. (D) Median behavior of hyperpolarized cells in G1 and with EA in G6 and the corresponding boxplot representation. (E) Median behavior of hyperpolarized cells both in G1 and in G6 and the corresponding boxplot representation. (F) Median behavior of cells with EA in G1 and depolarized in G6 and the corresponding boxplot representation. (G) Median behavior of hyperpolarized cells in G1 and depolarized in G6. (H) The behavior of the only three cells that were depolarized both in G1 and in G6.

able to reproduce the amplitude reduction observed experimentally. However, as in the previous case, we are not able to simulate the transition from EA to Hy. Finally, the rare depolarized cells in G1 maintain their state in G6 (3 cells, Figs. 3B and 3H).

Thus, simulating the glucose increase by decreasing the value of the KATP-channel conductance and increasing the value of the leak channel conductance, as performed in our recent paper (Montefusco & Pedersen (2015)), allows achieving the spike amplitude reduction experimentally observed; however, in this case, we note a consistent increase in the number of depolarized cells, with cells exhibiting EA or being silent in G1 becoming depolarized in G6 (Gromada et al. (2007); Le Marchand & Piston (2010)), while the experimentally observed repolarization is not obtained.

3.3. Simulating the effects of somatostatin by GIRK channel allows reproducing repolarization due to glucose increase

We investigate the role of somatostatin on the alpha-cell regulation by introducing a GIRK channel in the model (see Methods). Indeed, it has been shown that somatostatin secretion has an important role on alpha-cell activity by causing repolarization (Briant et al. (2016)) and glucagon inhibition (Strowski et al. (2000)) via GIRK channels at physiological glucose levels. Fig. 4 shows the alpha-cell population electrical behavior at G1 and G6 by simulating the glucose increase at G6 through a decrease of the KATP-channel conductance and an increase of the GIRK channel conductance (see Methods). The frequency of the three types of responses is significantly different between G1 and G6 ($p < 0.001$ by Madansky test of interchangeability) also in this scenario, which we call *case 3*.

In this case, from G1 to G6, we obtain an increase in the fraction of hyperpolarized cells due to the simulated somatostatin effect (see Figs. 4A and 4B). In particular, most of the cells exhibiting EA in G1 repolarize as experimentally observed in Briant et al. (2016) (504 of 770 cells, see Figs. 4B and 4E), while the remaining cells continue to show EA (266 of 770 cells, see Figs. 4B and 4C),

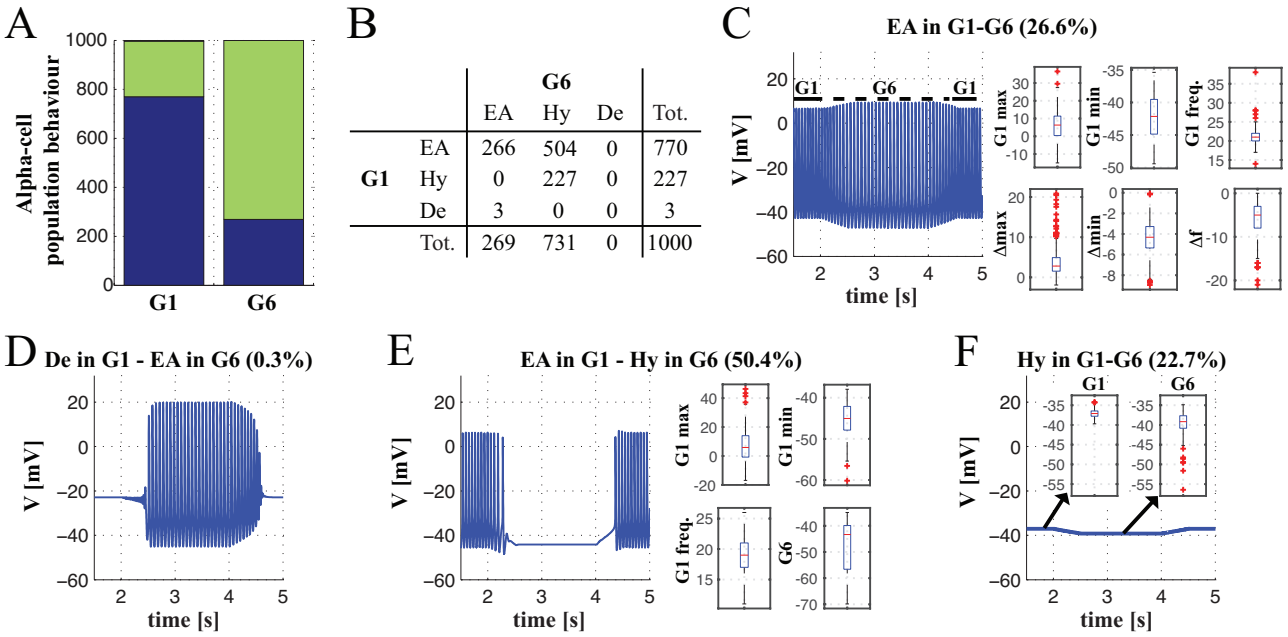

Figure 4: **Simulated electrical behavior of alpha-cell population at low (G1) and physiological (G6) glucose levels by reproducing the effects of somatostatin secretion thorough the modelling of the GIRK channel.** (A-B) Classification in terms of electrical behavior of the same population in Fig. 2 at G1 and G6 using the same criteria. (C) Median behavior of cells with EA both in G1 and in G6 and the corresponding boxplot representation. (D) Rare cases of depolarized cells in G1 and with EA in G6. (E) Median behavior of cells with EA in G1 and hyperpolarized in G6 and the corresponding boxplot representation. (F) Median behavior of hyperpolarized cells both in G1 and in G6 and the corresponding boxplot representation.

but without reproducing the experimental findings, i.e. the reduction in action potential peak voltage and the increase of the inter-spike membrane potential; on the contrary, we observe an increase of the median value of the peak and a decrease of the inter-spike membrane potential. The hyperpolarized cells in G1 maintain their silent state in G6 (227 cells, see Figs. 4B and 4F), while the rare depolarized cells in G1 initiate to exhibit EA in G6 (3 cells, see Fig. 4D).

Summarizing, simulating the glucose effect by decreasing the value of the KATP-channel conductance and introducing a GIRK current allows reproducing the experimental repolarization with cells exhibiting EA in G1 becoming silent in G6 (Barg et al. (2000); Manning Fox et al. (2006)). However, in this case we are not able to reproduce the spike amplitude reduction. Rather we note an increase of the spike peak and a decrease of the minimum for the cells exhibiting EA both in G1 and in G6.

3.4. Combining the intrinsic and paracrine mechanisms regulating alpha-cell activity reproduces the inhibitory effects produced by glucose increase

In order to reproduce the different inhibitory effects produced by glucose increase on alpha-cell electrical activity, i.e. action potential amplitude reduction or repolarization, we combine the intrinsic and paracrine mechanisms determining alpha-cell regulation at physiological glucose levels. In particular, we simulate the transition from G1 to G6 by decreasing the KATP-channel conductance and increasing the leak and GIRK channel conductances (see Methods); we call this scenario *case 4*. Figs. 5A and 5B show the simulated alpha-cell population behavior, which is differently distributed at G1 and G6 ($p < 0.001$ by Madansky test of interchangeability).

From G1 to G6, we note a reduction in the number of cells exhibiting EA with a corresponding increase of the fraction of hyperpolarized cells and a slight increase in the number of the depolarized cells (see Fig. 5B). In particular, $\sim$30% of cells exhibiting EA in G1 become hyperpolarized in G6 (227 of 770 cells, see Figs. 5B and 5F), reproducing spontaneous repolarization caused by somatostatin signaling (Briant et al. (2016)). A small number of cells with

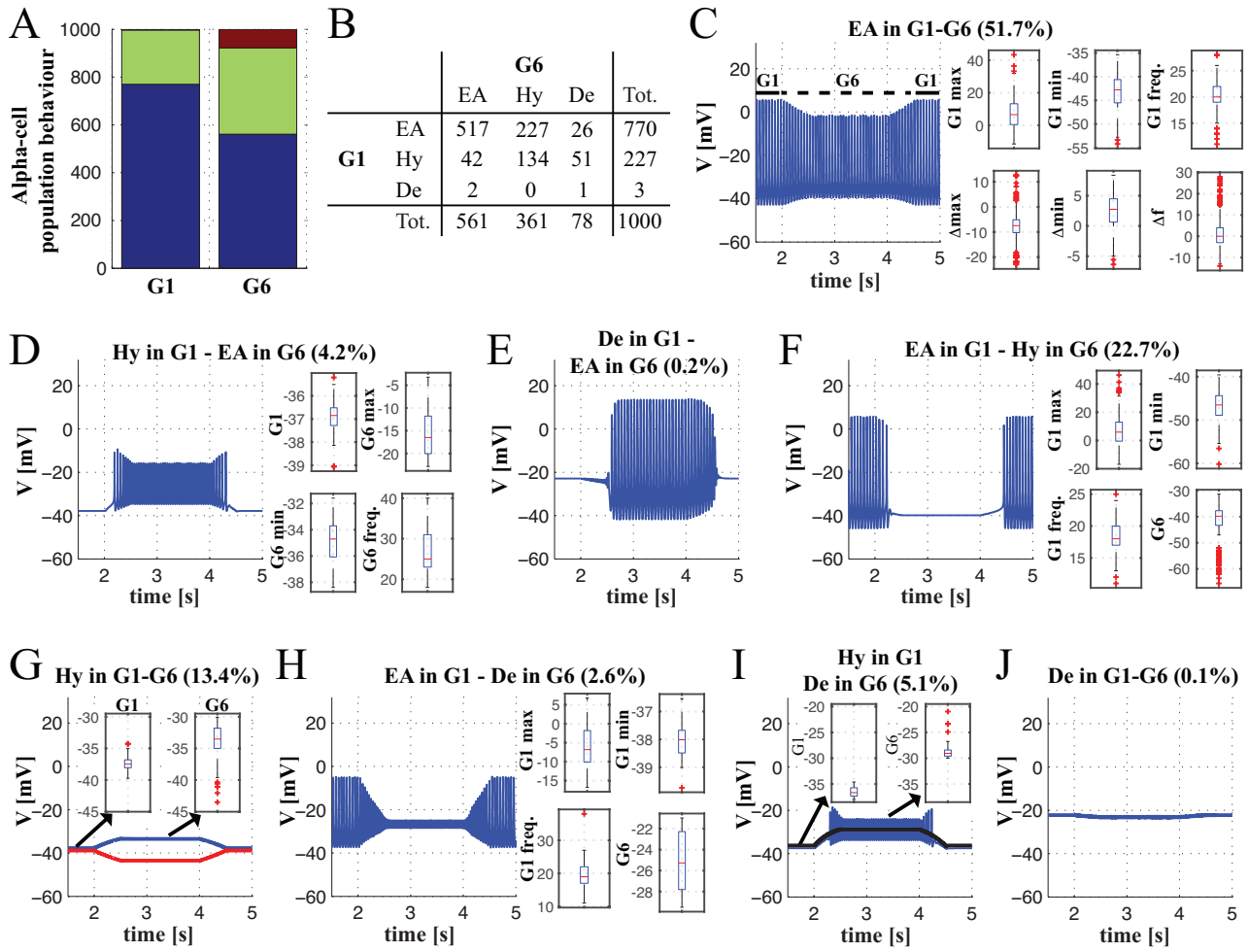

Figure 5: **Simulated electrical behavior of alpha-cell population at low (G1) and physiological (G6) glucose levels by combining intrinsic and paracrine mechanisms.** (A-B) Classification in terms of electrical behavior of the same population in Fig. 2 at G1 and G6 using the same criteria. (C) Median behavior of cells with EA both in G1 and in G6 and the corresponding boxplot representation. (D) Median behavior of hyperpolarized cells in G1 and with EA in G6 and the corresponding boxplot representation. (E) Rare depolarized cells in G1 and with EA in G6. (F) Median behavior of cells with EA in G1 and hyperpolarized in G6 and the corresponding boxplot representation. (G) Median behavior (blue curve) of hyperpolarized cells both in G1 and in G6 and the corresponding boxplot representation (the red curve shows the outliers behavior). (H) Median behavior of cells with EA in G1 and depolarized in G6 and the corresponding boxplot representation. (I) Median behavior of hyperpolarized cells in G1 and depolarized in G6 and the corresponding boxplot representation. (J) The only depolarized cell both in G1 and in G6.

EA in G1 become depolarized in G6 (26 of 770 cells, see Figs. 5B and 5H), while the remaining ∼67% of cells continue to exhibit electrical activity with a reduction of the action potential amplitude (median reduction ∼8 mV) as shown experimentally in Zhang et al. (2013) (517 of 770 cells, see Figs. 5B and 5C). A notable number of hyperpolarized cells in G1 maintains a silent state in G6 (134 of 227 cells, see Figs. 5B and 5G), while the remaining cells either become depolarized (51 of 227 cells, see Figs. 5B and 5I) or start to exhibit EA (42 of 227 cells, see Figs. 5B and 5D). Finally the rare depolarized cells in G1 either maintain their state in G6 (1 of 3 cells, see Figs. 5B and 5J) or initiate EA (2 of 3 cells, see Figs. 5B and 5E).

Therefore, by combining the intrinsic and paracrine mechanisms regulating alpha-cell activity, we are able to reproduce the two inhibitory effects of the glucose increase in the majority of cells, i.e. spikes with reduced amplitude with both a reduction in action potential peak voltage and an increase of the inter-spike membrane potential, or spontaneous repolarization caused by somatostatin signaling. Moreover, we also obtain apparently contrasting "outlier" responses with some cells becoming depolarized and generating APs at physiological glucose levels, as experimentally observed in Gromada et al. (2007); Le Marchand & Piston (2010). However, overall, the simulated alpha-cell population is less active and with reduced AP height, which would correspond to reduced glucagon secretion at the higher glucose concentration.

3.5. The results are valid also for another model

As explained in the Methods, we also simulated the electrical behavior of the alpha-cell population by using the parameter values for the activation and inactivation functions reported in the original alpha-cell model (Diderichsen & Göpel (2006)) (see Table 1), which were modified in the recent papers (Watts & Sherman (2014); Briant et al. (2017); Montefusco & Pedersen (2015)) with the aim to reduce spike frequency and increase its amplitude, in agreement with the experimental data. The results obtained from this set of parameters (see Supplementary Figs. S2 and S3), which describes the alpha-cell system named

model 2, are similar to those reported above (alpha-cell system named *model 1*).

For the alpha-cell population described by *model 2*, at G1 we obtain fewer cells exhibiting EA (36.6%), compared to the population characterized by *model 1* (77%). However, also for the population described by *model 2*, simulating the inhibitory glucose effect by decreasing only the KATP-channel conductance value does not allow reproducing the spike amplitude reduction. This reduction can be obtained by increasing the leak conductance value in G6 (see the first two rows of Supplementary Fig. S3). Also in this case, the repolarization caused by somatostatin is obtained by introducing a GIRK current and only combining the intrinsic and paracrine mechanisms (*case 4*) allows reproducing the two main inhibitory effects determined by the glucose increase (see the last two rows of Supplementary Figs. S2 and S3).

To investigate how robust our findings are to the choice of poorly characterized parameters, we performed additional simulations. For *case 4*, we obtained the population responses from both the models at G6 by increasing the leak conductance less (by 50% to $1.5\,\tilde{g}_L$) than the 100% increase (to $2\,\tilde{g}_L$) used in Fig. 5 (for *model 1*) and Figs. S2-S3 (for *model 2*). The results were similar to what we found by doubling the leak conductance, but with a tendency to less spike amplitude reduction for the cells with EA in both G1 and G6, due to the smaller increase in leak current (see Figs. S4 and S5 for *model 1* and *model 2*, respectively). We also found that fewer of the cells that were hyperpolarized in G1 became depolarized in G6 when the leak current, which tends to clamp the membrane potential at intermediate values due to the reversal potential for the leak current ($V_L = -25$ mV), is increased less when going from G1 to G6.

Finally, we vary the maximum value of the GIRK channel conductance for the populations described by both the models to investigate how sensitive our conclusions are to the choice of this value: decreasing its value leads to fewer cells showing repolarization in G6 (see the first two rows of Supplementary Figs. S6 and S7 for *model 1* and *2*, respectively), while the spike amplitude reduction is slightly increased (see the second row of Supplementary Figs. S8

and S9 for *model 1* and *2*, respectively); on the other hand, increasing its value results in more cells with EA in G1 and hyperpolarization in G6 (see the last two rows of Supplementary Figs. S6 and S7 for *model 1* and *2*, respectively), while the spike amplitude reduction is slightly decreased (see the last row of Supplementary Figs. S8 and S9 for *model 1* and *2*, respectively).

3.6. Predicting the role of membrane currents with regression analysis

We take advantage of the realistically generated synthetic alpha-cell population, which allows us to perform statistical analysis of the simulated results. In this way, we can investigate how the different membrane currents in the model contribute to the electrophysiological behavior at G1 and G6, and in particular, which model parameters are responsible for switching off electrical behavior by hyper- or depolarizing the cells.

For this scope, we performed multinomial logistic regression analyses on our sample of 1000 synthetic cells (obtained with *model 1, case 4*) for the two different glucose concentrations. The categorical response variable was the state (EA, Hy and De, see Methods). Presence/absence of A-type K^+ current, and log-transformed maximum current densities ($|I_{Na_{max}}|, |I_{LVACa_{max}}|, |I_{HVACa_{max}}|$), cell capacitance ($C_m$) and whole-cell input conductance density ($\tilde{G}$) entered as explanatory variables. After investigating also all possible statistical interactions between explanatory variables, we obtained final statistical models and report their results in Table 3. The analysis quantified the results by the log odds ratios (log OR), which estimate on logarithmic scale the relative effect of a 10% increase in a parameter value on the probability of cell being hyperpolarized (or depolarized) relative to having electrical activity, keeping all other parameters fixed.

First, we investigated how the model parameters influenced the three electrophysiological responses (EA, Hy, De) in G1. We found that an increase in C_m, I_{Na} and HVA Ca^{2+} currents promoted electrical activity compared to hyperpolarization. For example, a 10% increase in the membrane capacitance C_m, which in the model translates into smaller K^+ currents, reduces the probability of a

Table 3: **Estimated parameter effects in multinomial regression models.** Estimated log odds ratios for a 10% increase in the parameter value given with their standard errors in parentheses. For the indicator f_{KA} the estimated log odds ratios correspond to the effect of the presence compared to absence of A-type K^+ current. Interaction between covariates X and Y is indicated with the notation $X : Y$. Statistical significance is indicated as follows, with p-values from two-sided t-test: *: $0.01 < p \leq 0.05$; **: $0.001 < p \leq 0.01$; ***: $p \leq 0.001$.

Condition	G1	G6		G6 (only cells with EA in G1)	
Response	Hy	Hy	De	Hy	De
C_m	-4.60 (1.72)**	-1.66 (0.14)***	1.57 (0.28)***	-1.69 (0.16)***	3.40 (1.14)**
$\tilde{G}$	1.30 (1.00)	1.48 (0.28)***	2.49 (1.00)*	0.77 (0.33)*	5.25 (2.60)*
$\lvert I_{Na_{max}} \rvert$	-6.36 (2.46)**	-2.37 (0.34)***	-1.00 (0.57)	-1.95 (0.39)***	-3.35 (2.05)
$\lvert I_{HVACa_{max}} \rvert$	-8.96 (3.41)**	-1.99 (0.57)***	-1.62 (1.10)	-2.62 (0.72)***	-2.94 (3.03)
$\lvert I_{LVACa_{max}} \rvert$	0.99 (0.82)				
f_{KA}	7.66 (3.70)*	69.8 (19.2)***	51.6 (17.9)**		
$\tilde{G} : C_m$	2.08 (1.06)*				
$\tilde{G} : \lvert I_{LVACa_{max}} \rvert$	2.18 (0.98)*	0.15 (0.02)***	-0.06 (0.08)	0.26 (0.05)***	0.33 (0.41)
$\tilde{G} : \lvert I_{HVACa_{max}} \rvert$		0.14 (0.05)**	-0.42 (0.17)*		
$\tilde{G} : \lvert I_{Na_{max}} \rvert$		-0.46 (0.06)***	-0.08 (0.18)	-0.30 (0.07)***	-0.87 (0.53)
$\tilde{G} : f_{KA}$		1.26 (0.35)***	0.55 (0.41)		
$\lvert I_{Na_{max}} \rvert : f_{KA}$		-1.16 (0.36)**	-0.91 (0.31)**		
$\lvert I_{Na_{max}} \rvert : \lvert I_{HVACa_{max}} \rvert$		0.32 (0.12)**	0.33 (0.22)	0.32 (0.15)*	0.77 (0.62)
$\lvert I_{LVACa_{max}} \rvert : \lvert I_{HVACa_{max}} \rvert$				0.13 (0.06)*	0.21 (0.19)

cell being in state Hy, compared to being in EA, by 99% (OR $= e^{-4.60} = 0.01$, p-value $= 0.007$; Fig. 6A).

This relative probability was in contrast increased in presence of A-current I_{KA}. Increases in $\tilde{G}$, in interaction with C_m (notation $\tilde{G} : C_m$) and LVA Ca^{2+} currents ($\tilde{G} : \lvert I_{LVACa_{max}} \rvert$), increased the probability of a cell being hyperpolarized rather than showing electrical activity. Because of the presence of only 3 depolarized cells, we were unable to draw conclusions on how De depends on model parameters at G1.

For G6, similarly to G1, an increase in C_m, I_{Na} or HVA Ca^{2+} currents promoted electrical activity compared to hyperpolarization (Fig. 6B). Presence of A-current I_{KA} was associated to a higher probability of a cell being hyperpolarized, with respect to being in state EA, as was an increase in $\tilde{G}$. Moreover, jointly with presence of I_{KA}, or with LVA or HVA Ca^{2+} currents, an increase in $\tilde{G}$, slightly but significantly further increased the probability of a cell being

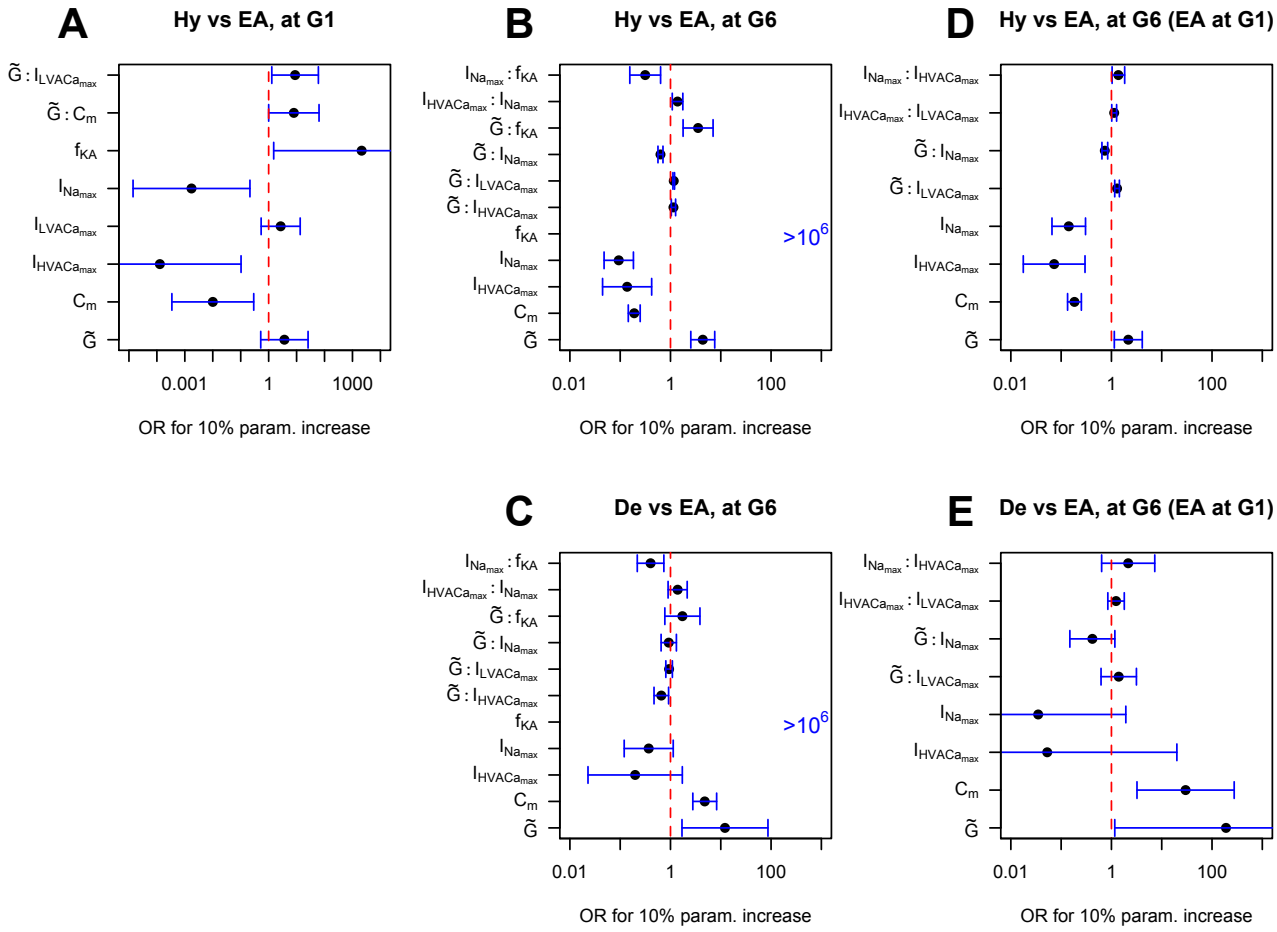

Figure 6: **Odds ratios (ORs) estimated with multinomial regression models.** In all panels, the vertical dashed line corresponds to OR=1, i.e., no estimated effect. Interaction between covariates X and Y is indicated by the notation X:Y. (A) Odds ratios and 95% confidence intervals for Hy versus EA at G1 for a 10% increase in parameter values, except for f_{KA} where the OR is for presence versus absence of I_{KA}. (B) As A, but at G6. (C) As B, but for De versus EA at G6. (D) As B, but restricted to the subpopulation exhibiting EA at G1. (E) As D, but for De versus EA.

hyperpolarized rather than showing electrical activity, whereas interaction between $\tilde{G}$ and I_{Na} promoted EA. I_{Na} also had significant interaction with I_{KA} promoting EA, whereas the interaction between I_{Na} and HVA Ca^{2+} currents is associated to a slightly higher probability of observing the cell being in state Hy.

In G6, depolarization compared to electrical activity was more likely with larger C_m, $\tilde{G}$, and in presence of A-current (Fig. 6C). However, in cells with A-current, I_{Na} promoted electrical activity, an effect that was not statistically significant in cells without I_{KA}. HVA Ca^{2+} currents promoted electrical activity but only in interaction with $\tilde{G}$. LVA Ca^{2+} currents did not significantly influence the probability of depolarization.

To understand which currents contribute to the cessation of electrical activity, either by hyperpolarizing or depolarizing the cell, when the glucose concentration is increased from G1 to G6, we restricted the analysis at G6 to the subgroup of cells that showed electrical activity in G1. Larger C_m, I_{Na} and HVA Ca^{2+} currents all significantly reduced the probability of the cell interrupting electrical activity in favor of hyperpolarization at G6. $\tilde{G}$ in contrast promoted hyperpolarization. Larger LVA Ca^{2+} currents in interaction with $\tilde{G}$ and HVA Ca^{2+} currents slightly increased the probability of hyperpolarization, as did the interaction between I_{Na} and HVA Ca^{2+} current and between I_{Na} and $\tilde{G}$. Depolarization at G6 was promoted by greater values of $\tilde{G}$ and C_m. Thus, interestingly a 10% increase in C_m (corresponding to smaller K^+ currents), is predicted to lower the number of hyperpolarized cells about 5-fold ($\text{OR} = e^{-1.69} = 0.18$; Fig. 6D) but to *increase* the probability of depolarization by a factor of 30 ($\text{OR} = e^{3.40} = 29.8$; Fig. 6E). In other words, *large* K^+ currents are predicted to have a negative effect on glucagon secretion by hyperpolarizing cells, but an even stronger positive impact by avoiding depolarization, likely by repolarizing cells sufficiently to reactivate action potential generating Ca^{2+} and Na^+ currents (Spigelman et al. (2010)).

4. Discussion

Single alpha-cells can show different and apparently contrasting responses at similar conditions. For example, in response to glucose, they can be depolarized (Gromada et al. (2004); Zhang et al. (2013)) or hyperpolarized (Barg et al. (2000); Manning Fox et al. (2006)), with a corresponding calcium response being positive (Le Marchand & Piston (2010)) or negative (MacDonald et al. (2007); Vieira et al. (2007)). These apparently conflicting results plausibly reflect the great heterogeneity within the alpha-cell population (Huang et al. (2011); Briant et al. (2017)) and, therefore, it is becoming clear that a single alpha-cell model with a single set of parameters is unable to explain the different electrophysiological responses at similar conditions. Here, we addressed these issues by assuming cell-to-cell variation through the exploitation of published single-cell data on the different currents and cell size (Huang et al. (2011); Briant et al. (2017)) in order to devise a computational model characterizing the heterogeneous alpha-cell population. In this way, each cell is not represented by an "average" alpha-cell, but by a random generation of the main electrophysiological parameters according to their experimental distributions (Huang et al. (2011); Briant et al. (2017)). This allowed us to predict the various electrophysiological responses that can be expected, and to reconcile contrasting experimental findings and interpretations of the direct effect of glucose on alpha-cells. Note that the alpha-cells are not electrically coupled as the beta-cells, where gap junction coupling helps to tame cell-to-cell heterogeneity (Smolen et al. (1993); Benninger et al. (2014)). However, there are paracrine signalling pathways that regulate alpha-cell activity, for example those mediated by somatostatin causing membrane repolarization with a resulting glucagon inhibition at physiological glucose levels (Briant et al. (2016)).

We showed that only combining intrinsic and paracrine factors allows us to reproduce the various effects produced by glucose increase (see Fig. 5): (i) reduction of the spike amplitude, determining less activation of Ca^{2+}channels involved in exocytosis (Zhang et al. (2013); MacDonald et al. (2007); Göpel

et al. (2000); Walker et al. (2011)), (ii) hyperpolarization (Briant et al. (2016); Barg et al. (2000); Manning Fox et al. (2006)), with resulting inhibition of glucagon release, or (iii) occasional depolarization of silent cells leading to AP generation and Ca^{2+} influx (Gromada et al. (2007); Le Marchand & Piston (2010)). Overall, in our simulations, the inhibitory effects produced by glucose increase prevailed over the other factors, resulting in reduced electrical activity at the population level, which would presumably lead to inhibition of glucagon secretion. Any reduction in electrophysiological activity in the alpha-cell population could be further enhanced e.g. by glucose-induced lowering of cAMP levels, which has been shown to be involved in inhibition of glucagon secretion (Tengholm & Gylfe (2017); Hughes et al. (2018); Yu et al. (2019)), but was not modeled here due to the poor understanding of the underlying mechanisms (Yu et al. (2019)). Similarly, we did not model Ca^{2+} dynamics in the cytosol and ER, which would be needed to include the contribution from any SOC current. We note that the electrophysiological properties of such a current are not well characterized in alpha-cells, but the SOC current should decrease when the glucose level is increased (Vieira et al. (2007); Liu et al. (2004)), in contrast to the increase in leak currents included here to simulate the increase in glucose. We propose that the leak current reflects e.g. SGLT2 mediated currents (Bonner et al. (2015); Pedersen et al. (2016)).

Table 2 indicates, for each of the four simulated cases, the parameter variations used for modeling glucose increase, and the simulated effects on the electrophysiological responses. We found that, generally, a reduction only in the KATP conductance is insufficient for reproducing the spike reduction due to the glucose increase at physiological levels, but an increase of the leak conductance value is needed (Montefusco & Pedersen (2015), see Figs. 2 and 3). However, the KATP and leak channel conductance variations describing the intrinsic mechanisms in response to glucose increase are unable to reproduce spontaneous repolarization, likely caused by somatostatin signaling. Introducing the GIRK current, which characterize the paracrine effects due to somatostatin, allows us to reproduce repolarization by glucose increase (see Fig. 4).

Another level of heterogeneity that we did not consider explicitly regards the glucose-sensitive mechanisms operating in the individual alpha-cells. It seems reasonable that some alpha-cells may rely mainly on KATP and leak channel mediated AP lowering (*case 2*; second row in Table 2), whereas others could be more sensitive to somatostatin released from neighboring delta-cells, and thus respond to glucose with hyperpolarization (*case 3*; third row on Table 2), for example because of their location in the islet. In other words, the alpha-cell population may be heterogeneous not only with respect to electrophysiological parameters, leading to diverse responses as indicated in the last three columns of Table 2, but may also be a mix of the mechanisms corresponding to the different rows. It will be interesting to see whether these distinctions will emerge in future studies using e.g. imaging of alpha-cells in their natural environment.

Using our synthetic alpha-cell population, we investigated the role of the different currents in shaping the electrophysiological responses using statistical regression models. We found that small variations in parameter values can have great influence on the fraction of cells showing a certain kind of electrophysiological behavior, as quantified by the odds ratios (Table 3), which reflects the delicate balance between currents in the mathematical model and, likely, in alpha-cells. Altogether, our analyses suggest that inward currents promote electrical activity compared to hyperpolarization, as expected. Larger values of $\tilde{G}$ and C_m respectively reduced and increased the propensity for EA compared to hyperpolarization. At 6 mM glucose, depolarization compared to electrical activity was more likely with higher values of $\tilde{G}$ and C_m.

Because of the way the model is generated, larger values of C_m correspond to smaller K^+ currents. Such smaller K^+ currents appeared to promote electrical activity rather than hyperpolarization, as could be expected, and found experimentally (Huang et al. (2013)). Moreover, smaller K^+ currents increased the probability of a cell being depolarized compared to exhibiting electrical activity, probably because large K^+ currents are needed to hyperpolarize the membrane sufficiently to allow reactivation of inwards Na^+ and Ca^{2+} currents underlying action potential firing (Spigelman et al. (2010)). A-type K^+ currents generally

promoted Hy and De compared to EA.

Our model approach splits the input conductance $\tilde{G}$ into K(ATP) and leak conductances, which have somewhat different effects. K(ATP) channels hyperpolarize the cells, and indeed we found that $\tilde{G}$ promoted Hy compared to EA. At 6 mM glucose, which is simulated by lowering the KATP-channel conductance and doubling the leak current, a larger value of $\tilde{G}$ results in more depolarizing current compared to 1 mM glucose. Indeed, $\tilde{G}$ promoted depolarization compared to EA at 6 mM glucose, likely due to more leak current, which tends to clamp the membrane potential at intermediate values since the reversal potential for the leak current was set to $V_L = -25$ mV.

We note that our approach is similar in spirit to studies considering electrophysiological heterogeneity in neurons and cardiac cells. For example, Goldman et al. (2001) and Fletcher et al. (2016) used parameter sweeping to find various patterns of electrical activity in model neurons and pituitary cells, respectively, and Fletcher et al. (2016) further performed bifurcation analyses to understand the underlying generating mechanisms. Similarly, Ori et al. (2018) investigated how parameter variation influences behavior of the Hodgkin-Huxley model, and showed that the behavior is largely determined by combination of what they called "structural" and "kinetic" parameters. In these works, the interest was mainly on determining where in parameter space transitions between qualitatively different kinds of behavior occurred. In contrast, we focused on the changes in behavior when the glucose concentration was raised, and how the presence or absence of these changes depend on the various individual parameters. In cardiac cells, Sobie (2009) used regression analysis to investigate how changes in parameter values influences e.g. action potential duration in cardiac model cells, an approach similar to our statistical analysis of the simulated alpha-cell population. However, we were interested in how parameters determine quantitatively different behavior (e.g. hyperpolarization vs. electrical activity) and consequently used multivariate logistic statistical analysis, whereas Sobie and co-workers use linear statistical modeling since e.g. the action potential duration is a continuous response variable of interest in cardiac cells (Sobie (2009);

Sarkar et al. (2012)).

5. Conclusion

In diabetes, glucagon secretion is malfunctioning with excessive release at physiological and high glucose concentrations, and a too little glucagon being secreted when the glucose concentration is low. Our analyses indicate that this type of behavior is seen, for example, when K^+ current density is increased (in our model this corresponds to C_m being reduced), since at higher glucose levels more K^+ current would increase action potential amplitude and glucose release, rather than depolarization and reduced secretion. In contrast, at low glucose concentrations larger K^+ current would interfere with electrical activity and lead to hyperpolarization and reduced secretion. Interestingly, various K^+ channels have been linked to disturbed glucagon secretion (Spigelman et al. (2010); Dadi et al. (2015); Engelbrechtsen et al. (2018)). We believe this kind of hypothesis-generating speculations illustrates the usefulness of our approach, and the kind of information that can be obtained only when considering cell-to-cell heterogeneity and with a combination of mathematical modeling and statistical analyses of the synthetic cell population.

6. Author Contributions

F.M. conceived mathematical modeling, implemented the mathematical model, prepared figures, and wrote the article. G.C. conceived and performed statistical analyses, and prepared statistical results, figure and methods. M.G.P. conceived research and wrote the article. All authors revised the article, and approved the final version.

7. Declaration of interest

Declarations of interest: none.

8. Acknowledgements

F.M. was supported by the University of Padova (Research Grant BIRD 2017). M.G.P. was supported by the University of Padova (Research Project SID 2017 and Research Project PROACTIVE 2018).

9. Supplementary Material

- A single .pdf file including the supplementary figures.
- A zipped folder containing the MATLAB code for generating the results presented in the main text and Supplementary Material.

10. References

Ashcroft, F. M., & Rorsman, P. (2012). Diabetes mellitus and the beta cell: The last ten years. *Cell*, *148*, 1160–1171. doi:10.1016/j.cell.2012.02.010.

Barg, S., Galvanovskis, J., Göpel, S. O., Rorsman, P., & Eliasson, L. (2000). Tight coupling between electrical activity and exocytosis in mouse glucagon-secreting alpha-cells. *Diabetes*, *49*, 1500–1510.

Benninger, R. K., & Hodson, D. J. (2018). New understanding of beta-cell heterogeneity and in situ islet function. *Diabetes*, *67*, 537–547. doi:10.2337/dbi17-0040.

Benninger, R. K., Hutchens, T., Head, W. S., McCaughey, M. J., Zhang, M., Marchand, S. J. L., Satin, L. S., & Piston, D. W. (2014). Intrinsic islet heterogeneity and gap junction coupling determine spatiotemporal ca2+ wave dynamics. *Biophysical Journal*, *107*, 2723–2733. doi:10.1016/j.bpj.2014.10.048.

Bonner, C., Kerr-Conte, J., Gmyr, V., Queniat, G., Moerman, E., Thévenet, J., Beaucamps, C., Delalleau, N., Popescu, I., Malaisse, W. J., Sener, A., Deprez, B., Abderrahmani, A., Staels, B., & Pattou, F. (2015). Inhibition of the

glucose transporter SGLT2 with dapagliflozin in pancreatic alpha cells triggers glucagon secretion. *Nature Medicine*, *21*, 512–517. doi:10.1038/nm.3828.

Briant, L., Salehi, A., Vergari, E., Zhang, Q., & Rorsman, P. (2016). Glucagon secretion from pancreatic alpha-cells. *Upsala Journal of Medical Sciences*, *121*, 113–119. doi:10.3109/03009734.2016.1156789.

Briant, L. J. B., Zhang, Q., Vergari, E., Kellard, J. A., Rodriguez, B., Ashcroft, F. M., & Rorsman, P. (2017). Functional identification of islet cell types by electrophysiological fingerprinting. *Journal of The Royal Society Interface*, *14*, 20160999. doi:10.1098/rsif.2016.0999.

Capozzi, M. E., Wait, J. B., Koech, J., Gordon, A. N., Coch, R. W., Svendsen, B., Finan, B., D'Alessio, D. A., & Campbell, J. E. (2019). Glucagon lowers glycemia when -cells are active. *JCI Insight*, *5*. doi:10.1172/jci.insight.129954.

Cappon, G., & Pedersen, M. G. (2016). Heterogeneity and nearest-neighbor coupling can explain small-worldness and wave properties in pancreatic islets. *Chaos: An Interdisciplinary Journal of Nonlinear Science*, *26*, 053103. doi:10.1063/1.4949020.

Cheng-Xue, R., Gomez-Ruiz, A., Antoine, N., Noel, L. A., Chae, H.-Y., Ravier, M. A., Chimienti, F., Schuit, F. C., & Gilon, P. (2013). Tolbutamide controls glucagon release from mouse islets differently than glucose: Involvement of katp channels from both alpha-cells and beta-cells. *Diabetes*, *62*, 1612–1622. doi:10.2337/db12-0347.

Croissant, Y. (2018). *mlogit: Multinomial Logit Models*. URL: https://CRAN.R-project.org/package=mlogit.

Dadi, P. K., Luo, B., Vierra, N. C., & Jacobson, D. A. (2015). Task-1 potassium channels limit pancreatic alpha-cell calcium influx and glucagon secretion. *Molecular endocrinology (Baltimore, Md.)*, *29*, 777–787. doi:10.1210/me.2014-1321.

D'Alessio, D. (2011). The role of dysregulated glucagon secretion in type 2 diabetes. *Diabetes Obes Metab*, *13 Suppl 1*, 126–132. URL: http://dx.doi.org/10.1111/j.1463-1326.2011.01449.x. doi:10.1111/j.1463-1326.2011.01449.x.

Diderichsen, P. M., & Göpel, S. O. (2006). Modelling the electrical activity of pancreatic alpha-cells based on experimental data from intact mouse islets. *J Biol Phys*, *32*, 209–29. doi:10.1007/s10867-006-9013-0.

Engelbrechtsen, L., Mahendran, Y., Jonsson, A., Gjesing, A. P., Weeke, P. E., Jørgensen, M. E., Færch, K., Witte, D. R., Holst, J. J., Jørgensen, T., Grarup, N., Pedersen, O., Vestergaard, H., Torekov, S., Kanters, J. K., & Hansen, T. (2018). Common variants in the herg (kcnh2) voltage-gated potassium channel are associated with altered fasting and glucose-stimulated plasma incretin and glucagon responses. *BMC genetics*, *19*, 15. doi:10.1186/s12863-018-0602-2.

Fletcher, P., Bertram, R., & Tabak, J. (2016). From global to local: exploring the relationship between parameters and behaviors in models of electrical excitability. *J Comput Neurosci*, *40*, 331–45. doi:10.1007/s10827-016-0600-1.

Goldman, M. S., Golowasch, J., Marder, E., & Abbott, L. F. (2001). Global structure, robustness, and modulation of neuronal models. *J Neurosci*, *21*, 5229–38.

Göpel, S. O., Kanno, T., Barg, S., Weng, X. G., Gromada, J., & Rorsman, P. (2000). Regulation of glucagon release in mouse alpha-cells by katp channels and inactivation of ttx-sensitive na+ channels. *J Physiol*, *528*, 509–520.

Gromada, J., Franklin, I., & Wollheim, C. B. (2007). Alpha-cells of the endocrine pancreas: 35 years of research but the enigma remains. *Endocr Rev*, *28*, 84–116. URL: http://dx.doi.org/10.1210/er.2006-0007. doi:10.1210/er.2006-0007.

Gromada, J., Ma, X., Høy, M., Bokvist, K., Salehi, A., Berggren, P.-O., & Rorsman, P. (2004). Atp-sensitive k+ channel-dependent regulation of glucagon release and electrical activity by glucose in wild-type and sur1-/- mouse alpha-cells. *Diabetes*, *53 Suppl 3*, S181–S189.

Gutierrez, G. D., Gromada, J., & Sussel, L. (2017). Heterogeneity of the pancreatic beta cell. *Frontiers in Genetics*, *8*. doi:10.3389/fgene.2017.00022.

Huang, Y.-C., Rupnik, M., & Gaisano, H. Y. (2011). Unperturbed islet alpha-cell function examined in mouse pancreas tissue slices. *J Physiol*, *589*, 395–408. URL: http://dx.doi.org/10.1113/jphysiol.2010.200345. doi:10.1113/jphysiol.2010.200345.

Huang, Y.-C., Rupnik, M. S., Karimian, N., Herrera, P. L., Gilon, P., Feng, Z.-P., & Gaisano, H. Y. (2013). In situ electrophysiological examination of pancreatic alpha cells in the streptozotocin-induced diabetes model, revealing the cellular basis of glucagon hypersecretion. *Diabetes*, *62*, 519–530. doi:10.2337/db11-0786.

Hughes, J. W., Ustione, A., Lavagnino, Z., & Piston, D. W. (2018). Regulation of islet glucagon secretion: Beyond calcium. *Diabetes Obes Metab*, *20 Suppl 2*, 127–136. doi:10.1111/dom.13381.

Kahn, S. E., Zraika, S., Utzschneider, K. M., & Hull, R. L. (2009). The beta cell lesion in type 2 diabetes: there has to be a primary functional abnormality. *Diabetologia*, *52*, 1003–1012. URL: http://dx.doi.org/10.1007/s00125-009-1321-z. doi:10.1007/s00125-009-1321-z.

Le Marchand, S. J., & Piston, D. W. (2010). Glucose suppression of glucagon secretion: metabolic and calcium responses from alpha-cells in intact mouse pancreatic islets. *J Biol Chem*, *285*, 14389–14398. URL: http://dx.doi.org/10.1074/jbc.M109.069195. doi:10.1074/jbc.M109.069195.

Lee, Y. H., Wang, M.-Y., Yu, X.-X., & Unger, R. H. (2016). Glucagon is

the key factor in the development of diabetes. *Diabetologia*, *59*, 1372–1375. doi:10.1007/s00125-016-3965-9.

Liu, Y.-J., Vieira, E., & Gylfe, E. (2004). A store-operated mechanism determines the activity of the electrically excitable glucagon-secreting pancreatic alpha-cell. *Cell Calcium*, *35*, 357–65. doi:10.1016/j.ceca.2003.10.002.

MacDonald, P. E., De Marinis, Y. Z., Ramracheya, R., Salehi, A., Ma, X., Johnson, P. R. V., Cox, R., Eliasson, L., & Rorsman, P. (2007). A k atp channel-dependent pathway within alpha cells regulates glucagon release from both rodent and human islets of langerhans. *PLoS Biol*, *5*, e143. URL: http://dx.doi.org/10.1371/journal.pbio.0050143. doi:10.1371/journal.pbio.0050143.

Manning Fox, J. E., Gyulkhandanyan, A. V., Satin, L. S., & Wheeler, M. B. (2006). Oscillatory membrane potential response to glucose in islet beta-cells: A comparison of islet-cell electrical activity in mouse and rat. *Endocrinology*, *147*, 4655–4663. doi:10.1210/en.2006-0424.

Montefusco, F., & Pedersen, M. G. (2015). Mathematical modelling of local calcium and regulated exocytosis during inhibition and stimulation of glucagon secretion from pancreatic alpha-cells. *The Journal of Physiology*, *593*, 4519–4530. doi:10.1113/jp270777.

Ori, H., Marder, E., & Marom, S. (2018). Cellular function given parametric variation in the hodgkin and huxley model of excitability. *Proc Natl Acad Sci U S A*, *115*, E8211–E8218. doi:10.1073/pnas.1808552115.

Pedersen, M. G., Ahlstedt, I., Hachmane, M. F. E., & Göpel, S. O. (2016). Dapagliflozin stimulates glucagon secretion at high glucose: experiments and mathematical simulations of human a-cells. *Scientific Reports*, *6*. doi:10.1038/srep31214.

Pedersen, M. G., Corradin, A., Toffolo, G. M., & Cobelli, C. (2008). A subcellular model of glucose-stimulated pancreatic insulin secretion. *Philosophical*

Transactions of the Royal Society A: Mathematical, Physical and Engineering Sciences, *366*, 3525–3543. doi:10.1098/rsta.2008.0120.

Pipeleers, D. G. (1992). Heterogeneity in pancreatic beta-cell population. *Diabetes*, *41*, 777–781. doi:10.2337/diab.41.7.777.

Quesada, I., Todorova, M. G., Alonso-Magdalena, P., Beltrá, M., Carneiro, E. M., Martin, F., Nadal, A., & Soria, B. (2006). Glucose induces opposite intracellular Ca2+ concentration oscillatory patterns in identified alpha- and beta-cells within intact human islets of langerhans. *Diabetes*, *55*, 2463–2469. URL: http://dx.doi.org/10.2337/db06-0272. doi:10.2337/db06-0272.

Quoix, N., Cheng-Xue, R., Mattart, L., Zeinoun, Z., Guiot, Y., Beauvois, M. C., Henquin, J.-C., & Gilon, P. (2008). Glucose and pharmacological modulators of ATP-sensitive k+ channels control [ca2+]c by different mechanisms in isolated mouse alpha-cells. *Diabetes*, *58*, 412–421. doi:10.2337/db07-1298.

R Core Team (2018). *A Language and Environment for Statistical Computing*. URL: https://www.R-project.org.

Rorsman, P., Braun, M., & Zhang, Q. (2012). Regulation of calcium in pancreatic alpha- and beta-cells in health and disease. *Cell Calcium*, *51*, 300–8. doi:10.1016/j.ceca.2011.11.006.

Rorsman, P., & Huising, M. O. (2018). The somatostatin-secreting pancreatic δ-cell in health and disease. *Nat Rev Endocrinol*, *14*, 404–414. doi:10.1038/s41574-018-0020-6.

Sarkar, A. X., Christini, D. J., & Sobie, E. A. (2012). Exploiting mathematical models to illuminate electrophysiological variability between individuals. *J Physiol*, *590*, 2555–67. doi:10.1113/jphysiol.2011.223313.

Smolen, P., Rinzel, J., & Sherman, A. (1993). Why pancreatic islets burst but single beta cells do not. the heterogeneity hypothesis. *Biophysical Journal*, *64*, 1668–1680. doi:10.1016/s0006-3495(93)81539-x.

Sobie, E. A. (2009). Parameter sensitivity analysis in electrophysiological models using multivariable regression. *Biophys J*, *96*, 1264–74. doi:10.1016/j.bpj.2008.10.056.

Spigelman, A. F., Dai, X., & MacDonald, P. E. (2010). Voltage-dependent k(+) channels are positive regulators of alpha cell action potential generation and glucagon secretion in mice and humans. *Diabetologia*, *53*, 1917–1926. doi:10.1007/s00125-010-1759-z.

Strowski, M. Z., Parmar, R. M., Blake, A. D., & Schaeffer, J. M. (2000). Somatostatin inhibits insulin and glucagon secretion via two receptor subtypes: An in Vitro study of pancreatic islets from somatostatin receptor 2 knockout mice1. *Endocrinology*, *141*, 111–117. doi:10.1210/endo.141.1.7263.

Svendsen, B., Larsen, O., Gabe, M. B. N., Christiansen, C. B., Rosenkilde, M. M., Drucker, D. J., & Holst, J. J. (2018). Insulin secretion depends on intra-islet glucagon signaling. *Cell Rep*, *25*, 1127–1134.e2. doi:10.1016/j.celrep.2018.10.018.

Tengholm, A., & Gylfe, E. (2017). camp signalling in insulin and glucagon secretion. *Diabetes Obes Metab*, *19 Suppl 1*, 42–53. doi:10.1111/dom.12993.

Vieira, E., Salehi, A., & Gylfe, E. (2007). Glucose inhibits glucagon secretion by a direct effect on mouse pancreatic alpha cells. *Diabetologia*, *50*, 370–379. URL: http://dx.doi.org/10.1007/s00125-006-0511-1. doi:10.1007/s00125-006-0511-1.

Walker, J. N., Ramracheya, R., Zhang, Q., Johnson, P. R. V., Braun, M., & Rorsman, P. (2011). Regulation of glucagon secretion by glucose: paracrine, intrinsic or both? *Diabetes Obes Metab*, *13 Suppl 1*, 95–105. URL: http://dx.doi.org/10.1111/j.1463-1326.2011.01450.x. doi:10.1111/j.1463-1326.2011.01450.x.

Watts, M., & Sherman, A. (2014). Modeling the pancreatic alpha-cell: dual

mechanisms of glucose suppression of glucagon secretion. *Biophys J*, *106*, 741–51. doi:10.1016/j.bpj.2013.11.4504.

Yu, Q., Shuai, H., Ahooghalandari, P., Gylfe, E., & Tengholm, A. (2019). Glucose controls glucagon secretion by directly modulating camp in alpha cells. *Diabetologia*, . doi:10.1007/s00125-019-4857-6.

Zhang, Q., Ramracheya, R., Lahmann, C., Tarasov, A., Bengtsson, M., Braha, O., Braun, M., Brereton, M., Collins, S., Galvanovskis, J., Gonzalez, A., Groschner, L. N., Rorsman, N. J., Salehi, A., Travers, M. E., Walker, J. N., Gloyn, A. L., Gribble, F., Johnson, P. R., Reimann, F., Ashcroft, F. M., & Rorsman, P. (2013). Role of KATP channels in glucose-regulated glucagon secretion and impaired counterregulation in type 2 diabetes. *Cell Metabolism*, *18*, 871–882. doi:10.1016/j.cmet.2013.10.014.

Zhu, L., Dattaroy, D., Pham, J., Wang, L., Barella, L. F., Cui, Y., Wilkins, K. J., Roth, B. L., Hochgeschwender, U., Matschinsky, F. M., Kaestner, K. H., Doliba, N. M., & Wess, J. (2019). Intra-islet glucagon signaling is critical for maintaining glucose homeostasis. *JCI Insight*, *5*. doi:10.1172/jci.insight.127994.